

Article

Single-Crystal Structure Analysis of Three Novel Iron(II) Coordination Polymers with Bridging 1,3,5-Tris((1*H*-1,2,4-triazol-1-yl)methyl)benzene

Aysenur Limon¹, Dustin N. Jordan¹, Till Strothmann¹, Laure P. Cuignet^{1,2}, Yann Garcia² 
and Christoph Janiak^{1,*} 

¹ Institut für Anorganische Chemie und Strukturchemie, Heinrich-Heine-Universität, 40204 Düsseldorf, Germany; aysenur.limon@uni-duesseldorf.de (A.L.); dustin.jordan@uni-duesseldorf.de (D.N.J.); till.strothmann@uni-duesseldorf.de (T.S.); laure.cuignet@sciensano.be (L.P.C.)

² Institute of Condensed Matter and Nanosciences, Molecular Chemistry, Materials and Catalysis (IMCN/MOST), Université Catholique de Louvain, 1348 Louvain-la-Neuve, Belgium; yann.garcia@uclouvain.be

* Correspondence: janiak@uni-duesseldorf.de

Abstract: Three novel iron(II) coordination polymers, namely [Fe(H₂O)₂(ttmb)₂](ClO₄)₂·4H₂O (**1**), [Fe(H₂O)₂(ttmb)₂](BF₄)₂·4H₂O (**2**) and [Fe(NCS)₂(ttmb)₂] (**3**), were synthesized with the linker 1,3,5-tris((1*H*-1,2,4-triazol-1-yl)methyl)benzene (ttmb). The single-crystal structures show that all three compounds form a double-chain structure with the adjacent iron atoms being bridged by two ttmb linkers. The iron(II) ions are octahedrally surrounded by four N4 donor atoms from the 1,2,4-triazol-1-yl groups of four different ttmb linkers which form an equatorial plane and two trans-coordinated aqua ligands in **1** and **2** or isothiocyanato ligands in **3** in the axial positions. In view of the neutral bridging ttmb linker, there is a non-coordinated counter-anion in **1** and **2** (ClO₄ and BF₄, respectively), and a coordinated NCS anion in **3**. Compounds **1** and **2** are isostructural. Interestingly, the ttmb linker only utilizes two of its three potentially coordinating triazole groups. All iron(II) coordination networks are colorless or have a light-yellow color, being indicative of the high-spin state.

Keywords: coordination polymers; coordination networks; triazole ligand; iron(II); self-assembly; hydrogen bonds



Citation: Limon, A.; Jordan, D.N.; Strothmann, T.; Cuignet, L.P.; Garcia, Y.; Janiak, C. Single-Crystal Structure Analysis of Three Novel Iron(II) Coordination Polymers with Bridging 1,3,5-Tris((1*H*-1,2,4-triazol-1-yl)methyl)benzene. *Crystals* **2023**, *13*, 1574. <https://doi.org/10.3390/cryst13111574>

Academic Editors: Pedro Netto Batalha and Simona Nica

Received: 25 September 2023

Revised: 27 October 2023

Accepted: 2 November 2023

Published: 7 November 2023



Copyright: © 2023 by the authors. Licensee MDPI, Basel, Switzerland. This article is an open access article distributed under the terms and conditions of the Creative Commons Attribution (CC BY) license (<https://creativecommons.org/licenses/by/4.0/>).

1. Introduction

According to the definition of the International Union of Pure and Applied Chemistry (IUPAC), a coordination polymer is a one-, two- or three-dimensional (1D, 2D or 3D) coordination compound consisting of repeating units [1–4]. Coordination polymers are often formed by self-assembly processes and are constructed from metal ions as connectors and organic ligands as linkers [5–7]. They can provide a wide range of topologies and structures [8–11]. Self-assembly describes a process in which the molecules arrange themselves into an ordered pattern based on interactions without external forces [6,12–17]. For the construction of 2D or 3D networks, tripodal ligands with three coordinating groups are attractive linkers to connect between three metal ions as a basis for higher dimensionality [18–24]. Triazole-based ligands are appropriate as linkers in coordination polymers since they can be deprotonated to the corresponding azolate anions in which the nitrogen atoms are strong donor atoms for d-metal ions [25–34]. Not only the dimensionality but also the stability of networks increases with the number of donor atoms and coordination sites [35]. The geometry of coordination polymers depends on the structure of the linker, and also depends on the presence of non-coordinating anions [36]. Particularly non-coordinating anions not only balance the charges of the complex, but they also function as templates [37–41]. A template provides an organized arrangement of atoms to achieve a specific linkage of

atoms [39,40]. In addition to the anions, solvent molecules can act as templates and control the arrangement of a network [31,42–48]. Depending on the size and properties of the anion, the effect on the geometry can vary [49,50]. Even if the anion is not coordinated to the metal ion, there are intermolecular interactions with the surrounding network [47], such as anion- π , hydrogen bonding or Lewis base–acid interactions [48,51]. Hydrogen bonds within the coordination network also have an influence on the structure [7,52].

Iron(II) compounds with an octahedral coordination geometry of six nitrogen donor ligands often exhibit spin crossover (SCO) behavior [53]. SCO describes the reversible transition between a high-spin (HS) and a low-spin (LS) state induced through temperature change, light radiation or variation in pressure [54]. The color and its change from nearly colorless for the HS compound to red–violet for the LS complex upon cooling offers a quick first diagnosis of the SCO effect without elaborate magnetic or Mößbauer studies. In the solid-state X-ray structure, Fe–N bond lengths also indicate the spin state. The Fe–N bond lengths typically range from 2.1 to 2.2 Å for HS, and from 1.8 to 2.0 Å for LS [55,56].

2. Materials and Methods

The used chemicals were all commercially obtained and no further purification was done (see Supplementary Materials, Section S1). The used water was deionized.

FT-IR measurements were carried out on a Bruker TENSOR 37 IR spectrometer (Bruker, Billerica, MA, USA) in ATR mode (Platinum ATR-QL, Diamond) in the range 500–4000 cm^{-1} . NMR spectra were collected with a Bruker Avance III—300 (Bruker, Billerica, MA, USA) (^1H : 300 MHz; $^{13}\text{C}\{^1\text{H}\}$: 75 MHz). Elemental analyses were measured on a PerkinElmer 2400 series II elemental analyzer (PerkinElmer, Waltham, MA, USA) (accuracy of 0.5%). Thermogravimetric analyses were carried out using a Netzsch TG209 F3 Tarsus (Netzsch, Selb, Germany) under nitrogen atmosphere with a ramp of 5 K min^{-1} up to 1000 °C. X-ray powder diffraction measurements were performed on a Rigaku Mini-Flex600 (Rigaku, Tokyo, Japan) (600 W, 40 kV, 15 mA) at room temperature with Cu-K α radiation ($\lambda = 1.54184$ Å). The low-background silicon holder in the PXRD device is the cause of the rising baseline below 5° 2Theta. The highest reflex was normalized to 1. The simulated powder patterns were derived from the single crystal data using the MERCURY 2020.3.0 software [57].

Three novel iron(II) coordination polymers, namely $[\text{Fe}(\text{H}_2\text{O})_2(\text{ttmb})_2](\text{ClO}_4)_2 \cdot 4\text{H}_2\text{O}$ (compound 1), $[\text{Fe}(\text{H}_2\text{O})_2(\text{ttmb})_2](\text{BF}_4)_2 \cdot 4\text{H}_2\text{O}$ (compound 2) and $[\text{Fe}(\text{NCS})_2(\text{ttmb})_2]$ (compound 3), were synthesized with the linker 1,3,5-tris((1*H*-1,2,4-triazol-1-yl)methyl)benzene (ttmb) (see Section 2.1). Under a polarized-light Leica M80 microscope (Leica, Wetzlar, Germany), suitable single crystals were carefully selected and covered with oil on a cryo-loop. The single crystal diffraction measurement for compounds 1 and 3 were carried out on a Rigaku XtaLAB Synergy S diffractometer (Rigaku, Tokyo, Japan) with a hybrid pixel array detector and a micro-focus sealed X-ray tube, PhotonJet copper X-ray source ($\lambda = 1.54184$ Å). For cell refinement, data reduction and absorption correction CRYCALISPRO was used [58]. For compound 2, the measurement was performed on a Bruker Kappa APEX2 CCD X-ray diffractometer (Bruker, Billerica, MA, USA) with a microfocus sealed tube molybdenum X-ray source ($\lambda = 0.71073$ Å) and a multi-layer mirror monochromator. Cell refinement was performed with APEX2, data reduction with SAINT and adsorption correction with SADABS [59–61]. The crystal structures for compounds 1–3 were solved using OLEX2 with SHELXT and the refinement was done with SHELXL [62–64]. The graphics were drawn with the DIAMOND 4.0 software [65].

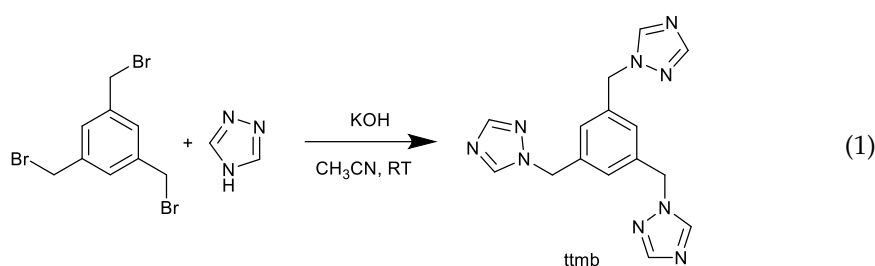
Photophysical measurements were performed on a fluorescence spectrophotometer Edinburgh Instrument FS5 (Edinburgh Instruments Ltd., Edinburgh, UK). The excitation and emission spectra were measured with a 150 W continuous xenon lamp as a light source.

Electrochemical measurements were conducted on an Interfere 1010E potentiostat (Gamry Instruments, Warminster, PA, USA) with an RRDE-3A station (ALS, Tokyo, Japan). A three-electrode setup was used with Ag/AgCl (stored in 3.5 mol L^{-1} KCL solution) as the reference electrode, platinum as the counter electrode and a glassy carbon electrode

(5 mm diameter) as the working electrode. A nitrogen-saturated acetonitrile solution with tetrabutylammonium hexafluorophosphate (0.1 mol L^{-1}) served as the electrolyte. The ink was prepared by dispersing 1 mg of the sample in 0.5 mL ethanol and 20 μL Nafion followed by sonication for 30 min. An amount of 10 μL of ink was dropped onto the working electrode and dried at 150 rpm for a loading of about $10 \mu\text{g cm}^{-2}$. The cyclic voltammograms were then recorded in the range from $-2.5 \text{ V vs. Ag/AgCl}$ to $1.3 \text{ V vs. Ag/AgCl}$ with a scan rate of 100 mV s^{-1} .

2.1. Synthesis

2.1.1. Synthesis of 1,3,5-Tris((1H-1,2,4-triazol-1-yl)methyl)benzene (ttmb)



The linker ttmb was synthesized with a modified synthesis procedure of Shang et al. [66] as shown in Equation (1). An amount of 0.85 g (12.3 mmol) of 1,2,4-triazole and 1.32 g (23.5 mmol) of potassium hydroxide were stirred in 30 mL of acetonitrile for 30 min at room temperature. Afterwards, a solution of 1.0 g (2.8 mmol) of 1,3,5-tris(bromomethyl)benzene in 20 mL of acetonitrile was added. The resulting solution was stirred for an additional 30 min at room temperature. After filtration, the solvent was removed in vacuo. Next, the resulting oil was dissolved in 20 mL of deionized water and extracted with chloroform ($5 \times 50 \text{ mL}$). Once the organic phase was dried with MgSO_4 , the solvent was again removed using rotatory evaporation. The product crystallized overnight and was then dried in vacuum at $60 \text{ }^\circ\text{C}$. Yield: 0.45 g (46%). $\text{C}_{15}\text{H}_{15}\text{N}_9$: calc. C 56.1, H 4.7, N 39.2; exp. C 55.5, H 4.6, N 38.5%. IR: $\tilde{\nu}$ [cm^{-1}]: 3114, 3096, 3034, 2994, 2955, 3034, 2993, 2956, 2849, 1798, 1757, 1711, 1609, 1503, 1466, 1445, 1430, 1373, 1338, 1298, 1270, 1207, 1170, 1137, 1096, 1018, 987, 960, 917, 895, 880, 858, 800, 742, 680, 648, 601, 570. $^1\text{H-NMR}$ (300 MHz, DMSO-d_6): δ [ppm]: 8.63 (s, 3H), 7.97 (s, 3H), 7.12 (s, 3H), 5.39 (s, 6H). $^{13}\text{C}\{^1\text{H}\}$ -NMR (75 MHz, DMSO-d_6): δ [ppm]: 151.81, 144.31, 137.26, 51.62.

2.1.2. Synthesis of $[\text{Fe}(\text{H}_2\text{O})_2(\text{ttmb})_2](\text{ClO}_4)_2 \cdot 4\text{H}_2\text{O}$ (Compound 1)

Please note that perchlorates are potentially explosive and should be handled with care! TGA shows an explosion at around $200 \text{ }^\circ\text{C}$ after the sample was dried at $60 \text{ }^\circ\text{C}$ in vacuo beforehand. An amount of 49 mg (0.19 mmol) of $\text{Fe}(\text{ClO}_4)_2 \cdot x\text{H}_2\text{O}$ and 84 mg (0.26 mmol) of ttmb were dissolved in 3 mL of H_2O and stored in a pre-heated oven at $60 \text{ }^\circ\text{C}$ for 20 h. After cooling down to room temperature over a period of 4 h, yellow crystals were obtained. The crystals were washed with water ($3 \times 3 \text{ mL}$) and stored in H_2O . Yield: 73 mg (38%). $\text{C}_{30}\text{H}_{42}\text{Cl}_2\text{FeN}_{18}\text{O}_{14}$: calc. C 40.2, H 3.4, N 28.0; exp. C 39.5, H 3.6, N 27.8%. IR: $\tilde{\nu}$ [cm^{-1}]: 3509, 3455, 3357, 3269, 3126, 3036, 2357, 1767, 1679, 1632, 1612, 1517, 1466, 1438, 1373, 1359, 1340, 1302, 1283, 1218, 1179, 1163, 1134, 1078, 1026, 989, 977, 962, 915, 886, 853, 778, 765, 747, 693, 677, 654, 621, 577.

2.1.3. Synthesis of $[\text{Fe}(\text{H}_2\text{O})_2(\text{ttmb})_2](\text{BF}_4)_2 \cdot 4\text{H}_2\text{O}$ (Compound 2)

For the synthesis of compound 2, two solutions were prepared. The first solution contained 122.1 mg (0.36 mmol) of $\text{Fe}(\text{BF}_4)_2 \cdot 6\text{H}_2\text{O}$ and 62.9 mg (0.36 mmol) of ascorbic acid in 1.5 mL of H_2O . The second solution was composed of 57.9 mg (0.18 mmol) of ttmb dissolved in 1.5 mL of EtOH. Both solutions were heated up to $80 \text{ }^\circ\text{C}$ and then combined. The mixture was stored in the preheated oven at $60 \text{ }^\circ\text{C}$ for 24 h and cooled down for 4 h. The resulting colorless crystals were washed with a 1:1 (v:v) mixture of H_2O :EtOH ($3 \times 3 \text{ mL}$)

and later stored in that mixture as well. Yield: 68.5 mg (56%). $C_{30}H_{42}B_2F_8FeN_{18}O_{14}$: calc. C 36.8, H 4.3, N 25.8; exp. C: 36.9, H 4.2, N 25.4%. IR: $\tilde{\nu}$ [cm^{-1}]: 3537, 3460, 3264, 3129, 3033, 2360, 1766, 1634, 1612, 1518, 1469, 1439, 1374, 1360, 1341, 1284, 1218, 1180, 1163, 1144, 1133, 1047, 1023, 990, 977, 913, 884, 852, 795, 778, 765, 747, 693, 677, 654, 577.

2.1.4. Synthesis of $[Fe(NCS)_2(ttmb)_2]$ (Compound 3)

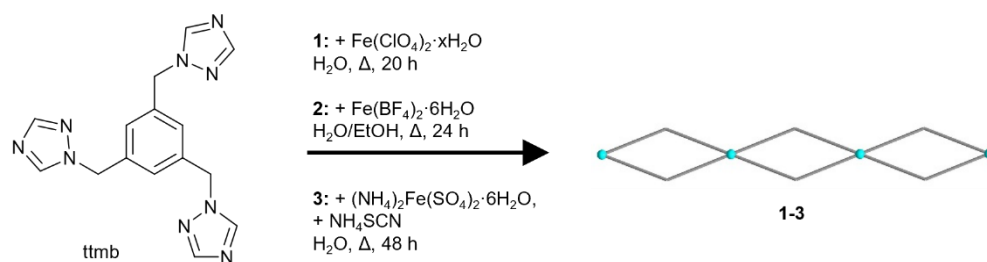
A modified procedure of Garcia et al. [67] was used. Three solutions were prepared. Solution 1 contained 19.6 mg (0.05 mmol) of $(NH_4)_2Fe(SO_4)_2 \cdot 6H_2O$ and 32 mg (0.18 mmol) of ascorbic acid in 1 mL of H_2O . The second solution contained 7 mg (0.09 mmol) of NH_4SCN in 1 mL H_2O . Solution 3 was composed of 29 mg (0.09 mmol) of ttmb in 1 mL of deionized water. After heating each solution near its boiling point, solution 2 was added to solution 1. Solution 3 was then added dropwise to this combined solution. After 48 h at 60 °C, colorless crystals were obtained. The crystals were washed with water (3×3 mL) and stored in H_2O . Yield: 26 mg (65%). $C_{32}H_{30}FeN_{20}S_2$: calc.: C = 47.2, H = 3.7, N = 34.4; exp.: C = 46.5, H = 3.8, N = 33.9. IR: $\tilde{\nu}$ [cm^{-1}]: 3580, 3436, 3140, 3126, 3110, 2961, 2845, 2338, 2162, 2046, 1779, 1757, 1611, 1522, 1502, 1466, 1430, 1359, 1340, 1311, 1298, 1275, 1202, 1178, 1159, 1131, 1019, 988, 974, 956, 923, 884, 847, 789, 759, 747, 682, 673, 652, 633, 583, 569.

3. Results and Discussion

The linker 1,3,5-tris((1*H*-1,2,4-triazol-1-yl)methyl)benzene (ttmb) was synthesized by a nucleophilic substitution reaction between 1*H*-1,2,4-triazole and 1,3,5-tris(bromomethyl)benzene in acetonitrile (see Equation (1)). The authentication was done by 1H , ^{13}C NMR and IR spectroscopy. The thermogravimetric analysis of the free ttmb linker shows a thermal stability up to 310 °C. There is a sudden mass loss until 380 °C, which accounts for more about 50% of the initial mass (see Supplementary Materials, Figure S7, Section S2). The excitation and emission spectra of ttmb were recorded at room temperature in the solid phase and are given in the Supplementary Materials S8, Figure S14. The linker ttmb shows an excitation maximum at 420 nm in the visible region. The emission spectrum has its maximum at around 360 nm upon excitation at 320 nm.

A schematic presentation of the synthesis of the complexes 1–3 is given in Scheme 1. The compounds had to be prepared with different molar metal:ligand ratios, which were optimized beforehand, in order to obtain crystals of sufficient quality for single-crystal X-ray analysis. The molar M:L ratio for compound 1 was 2:3, for compound 2 it was 2:1 and for compound 3 it was 1:2. The synthesis for the crystals of 1 was carried out by combining the metal salt and the linker in water. For compound 2, the preparation was different: Two separate warm solutions were assembled and later combined. The first solution contained the metal salt with ascorbic acid and the second one contained the linker. This approach was chosen to avoid rapid precipitation as powders. A similar synthesis was done for 3. Additionally, a third warm solution with NH_4NCS was prepared and in order to form the intermediate product, ferrous nitrate; the solution of the metal salt and ascorbic acid were combined with this solution first, and then the solution of the linker was added [68]. The crystals have a colorless or a light-yellow color; microscopic images of the crystals can be found in the Supplementary Materials, Section S5.

The IR spectra of the coordination polymers 1–3 (see Supplementary Materials, Section S3) show their indicative bands for the ttmb linker at around 977 cm^{-1} for $\nu(C=C)$ and 1519 cm^{-1} for $\nu(C=N)$. Additionally, the characteristic bands for the anions of the compounds can be detected for the ClO_4^- of 1 at $\nu(Cl-O) = 621$ cm^{-1} , 1078 cm^{-1} . The band of the anion BF_4^- of 2 can be observed at $\nu(B-F) = 1047$ cm^{-1} and the anion of 3 at $\nu(NCS) = 2046$ cm^{-1} [69].



Scheme 1. Schematic presentation of the synthesis of the coordination polymers 1–3 with their double-chain structures. The blue spheres represent Fe(II) atoms.

Thermogravimetric analysis of compounds **1** and **2** revealed a gradual decomposition (at a heating rate of 5 K min^{-1} , see Supplementary Materials, Section S4). It starts at around $70 \text{ }^\circ\text{C}$ due to the loss of crystal water which for both complexes accounts for a mass loss of 13 wt.%. The theoretical water content in compounds **1** and **2** amounts to 12.4 wt.% for the four water molecules of crystallization and the two aqua ligands per formula unit. The main decomposition starts for compound **1** at $190 \text{ }^\circ\text{C}$ and for **2** at $250 \text{ }^\circ\text{C}$. Compound **1** decomposes almost completely with a mass loss of 84 wt.% in the second step, leaving a residual mass of only 3% at $600 \text{ }^\circ\text{C}$. Compound **2**, on the other hand, leaves a residual mass of 35% at $600 \text{ }^\circ\text{C}$. This suggests a higher thermal stability due to the BF_4 counter-anion. Compound **3**, which does not contain solvent of crystallization, is thermally stable up to $300 \text{ }^\circ\text{C}$, where the decomposition of the ligand starts. At $1000 \text{ }^\circ\text{C}$, a residual mass of 11 wt.% remains (Figure S10), similar as in the TGA of the free ttmb linker (Figure S7).

The experimental powder X-ray diffraction patterns of **1–3** could be positively matched to the simulated pattern from the single-crystal X-ray analysis which indicated a high phase purity for the crystalline part of each compound (Figure 1). In addition, all X-ray diffraction patterns show great agreement with the simulation. At the same time, light microscopy images of the batches of compounds **1–3** showed almost exclusively crystalline matter (see Supplementary Materials, Section S5).

The emission spectra of compounds **1–3** were recorded in solid phase at room temperature. The samples were excited at $\lambda_{\text{exc}} = 320 \text{ nm}$ but did not exhibit any emission in the visible region (see Supplementary Materials, Section S8). From the very light-yellow color of compound **1** and colorless compounds **2** and **3**, there is also no significant absorption in the visible region, in agreement with the low-energy d-d splitting of high-spin $d^6\text{-Fe(II)}$ where the absorption will lie in the near-infrared region (NIR).

The similar cyclic voltammograms of the coordination polymers are shown in Figure 2. All three compounds have three anodic and two clearly visible cathodic potentials, which are indicative of three redox reactions. The potential of the Ag/AgCl reference electrode of 0.2 V has to be added to the measured potential for comparison to the standard redox potentials versus the standard hydrogen electrode (SHE). Note that here the electrochemical measurements were performed in acetonitrile whereas the standard redox potentials E° vs. SHE are based on aqueous solutions. The oxidation wave with $E_{\text{pa}} \approx 0.50 \text{ V}$ vs. Ag/AgCl or 0.7 V vs. SHE is assigned to the oxidation of Fe(II) to Fe(III) ($E^\circ = 0.77 \text{ V}$ in water, $\text{pH} = 0$). Upon reversal of the potential there is only a very small and not well developed peak for the reduction of Fe(III) to Fe(II) at $E_{\text{pc}} \approx 0.5 \text{ V}$. This suggests a nearly irreversible oxidation with an unstable Fe(III) compound. The two reduction potentials at $E_{\text{pc}} \approx -0.95 \text{ V}$ and $\approx -1.6 \text{ V}$ together with their oxidation potentials at $E_{\text{pa}} \approx -1.2 \text{ V}$ (shoulder) and $\approx -0.6 \text{ V}$, respectively (all values vs. Ag/AgCl), are then due to ligand redox processes.

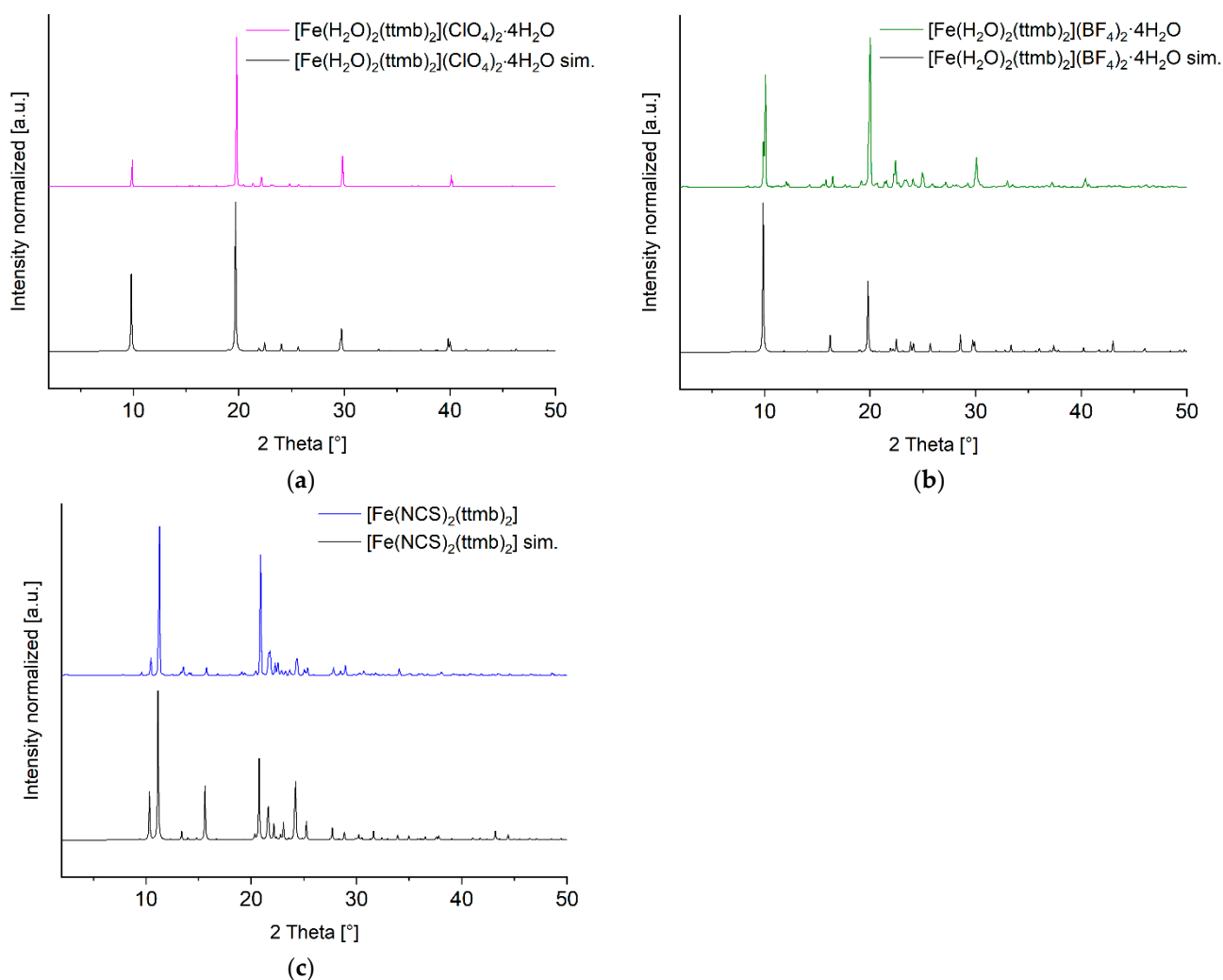


Figure 1. Powder X-ray diffraction patterns of compounds 1–3 as (a), (b) and (c), respectively, compared to their simulation. (Preferred orientation: 1: $h = -7, k = 0, l = -6$, March-Dollase = 10; 2: $h = -6, k = 0, l = -3$, March-Dollase = 5; 3: $h = -2, k = 8, l = -16$, March-Dollase = 3).

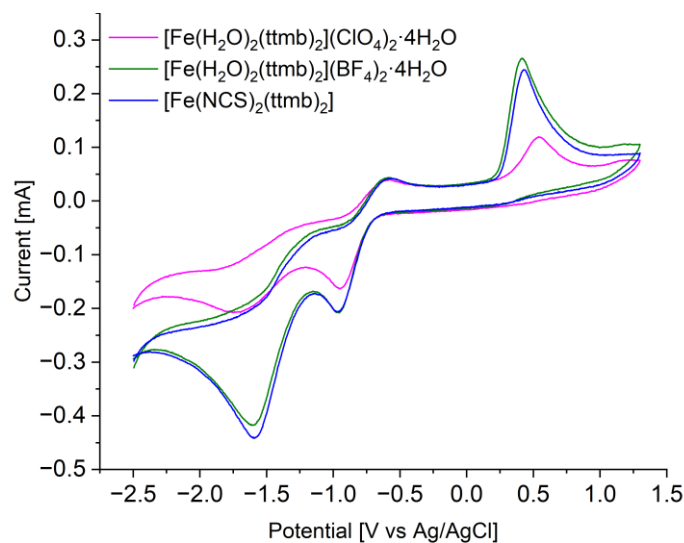


Figure 2. Cyclic voltammograms of compounds 1–3 (pink = 1, green = 2, blue = 3) spin-coated onto a glassy carbon electrode at $T = 293 \text{ K}$.

3.1. Crystal Structure of $[Fe(H_2O)_2(ttmb)_2](X)_2 \cdot 4H_2O$ (1: $X = ClO_4^-$; 2: $X = BF_4^-$)

Single-crystal X-ray analysis reveals that the isostructural complexes **1** and **2** crystallize in the monoclinic space group $P2_1/n$. The asymmetric unit consists of one half of an Fe(II) atom (on an inversion center), one ttmb ligand, one coordinated and two uncoordinated water molecules, and one uncoordinated ClO_4^- or BF_4^- anion (Figure 3). Due to the steric hindrance of the ttmb ligand and the interactions with the anions, the metal center possesses a somewhat distorted octahedral geometry with a FeO_2N_4 coordination environment (see Supplementary Materials, Section S7).

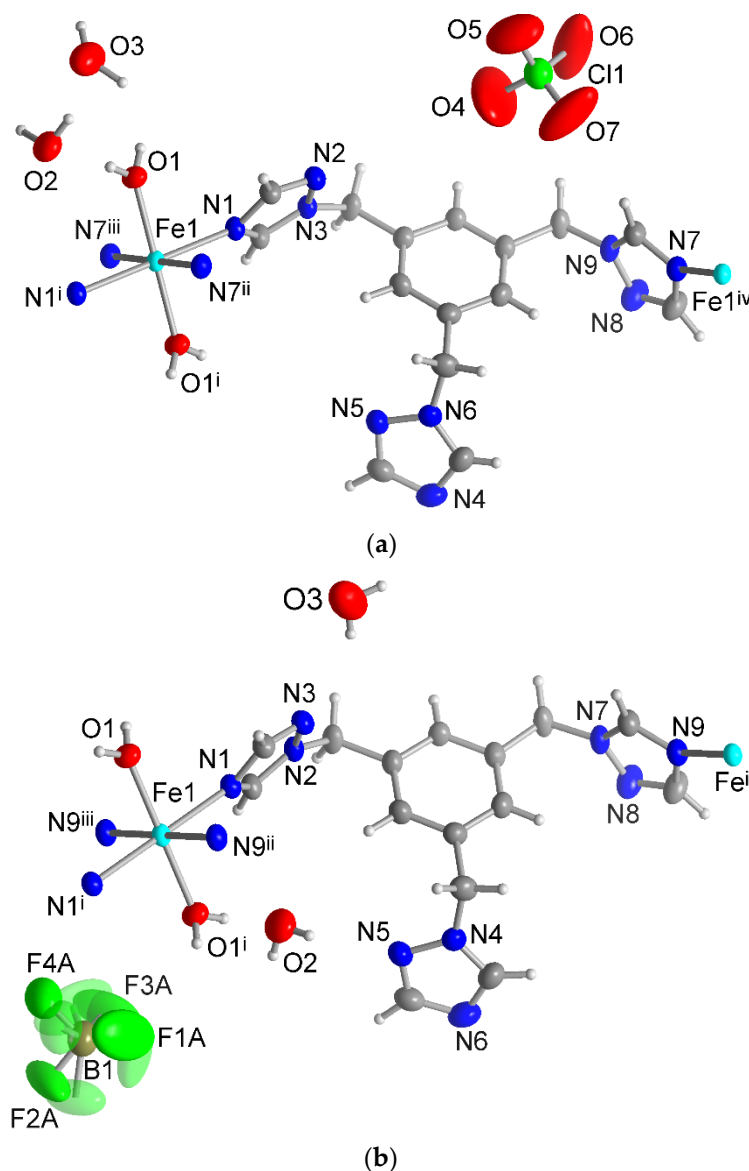


Figure 3. Extended asymmetric unit of compounds (a) **1** and (b) **2** (50% thermal ellipsoids and H atoms with arbitrary radii). The disordered F atoms of the BF_4^- anion of compound **2** are presented as transparent atoms. Symmetry transformation: (a): i = $-x + 1, -y + 1, -z$; ii = $-x + 1, -y + 1, -z + 1$; iii = $x, y, z - 1$; iv = $x, y, z + 1$. (b): i = $-x + 2, -y + 1, -z + 2$; ii = $-x + 2, -y + 1, -z + 1$; iii = $x, y, z + 1$.

The equatorial positions are occupied by four nitrogen atoms which are provided by four triazole groups of four ttmb units. The oxygen atoms of the water molecules are trans-positioned around the Fe(II) atom (Figure 3).

For compounds **1** and **2**, the Fe–N bond distances range from 2.08 to 2.22 Å. The Fe–N bond lengths in compound **3** lie between 2.07 and 2.23 Å. These bond lengths also indicate

that the Fe(II) centers in these compounds are in the high-spin state since the low-spin state complexes typically have shorter Fe–N bonds (within 1.8 to 2.0 Å) [55]. In addition, the light yellow color of complex **1** and the colorless compounds **2** and **3** signal an HS state, with LS state Fe(II) complexes having a red–violet color [55]. The spin-allowed d–d transitions of HS Fe(II) complexes lie in the near infrared (NIR), giving the complexes their off-white color, whereas the stronger ligand field in the LS Fe(II) complexes has the $^1A_{1g} \rightarrow ^1T_{1g}$ and $^1T_{2g}$ d–d transition at about 500 nm in the green absorption range so that the complexes appear red–violet [70]. The Fe–O length is about 2.07 Å for **1** and 2.08 Å for **2**.

Every ttmb ligand functions as a twofold bridge and connects two Fe(II) atoms with an anti-conformation of the coordinating triazole groups. The spanned distance between the Fe atoms is 13.46 Å. Every Fe(II) atom is connected to its neighbor by two ttmb linkers in a double-chain structure (Figure 4). Since the perchlorate and tetrafluoroborate anions have similar sizes, similar geometries and also similar chemical hardness, it was expected that both compounds **1** and **2** are isostructural [71]. The ionic radius of ClO_4^- is 2.37 Å, and that of BF_4^- is 2.29 Å [36].

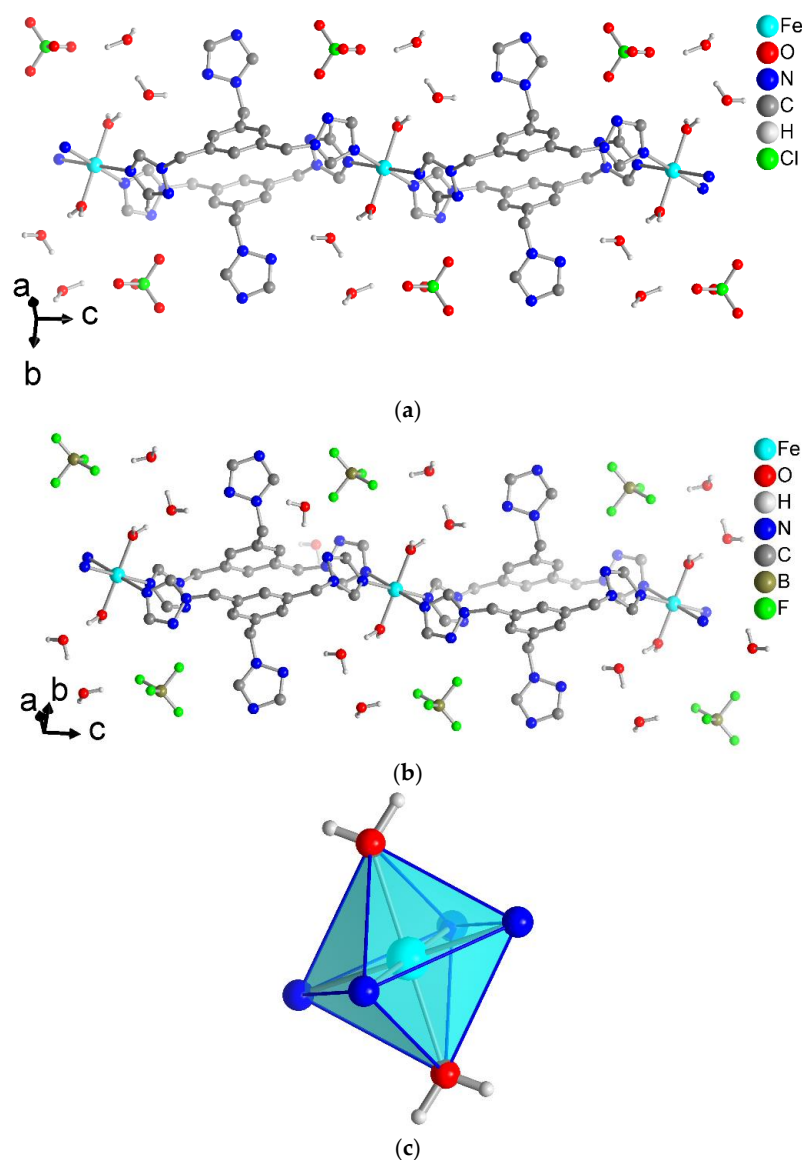


Figure 4. View of the double chain of compounds (a) **1** and (b) **2** with the surrounding crystal water and anions. For clarity, the H atoms have been omitted on the ttmb linkers. (c) Presentation of the octahedral iron(II) environment in **1** (identical to **2**).

The ClO_4^- and BF_4^- anions have $\text{C-H}\cdots\text{O}$ and $\text{C-H}\cdots\text{F}$, respectively, hydrogen bond interactions from the triazole groups of the ttmb linker [72]. For compound **1**, Figure 5 shows that a ClO_4^- anion interacts with one C–H of each triazole ring of the ttmb linker. For the $\text{C-H}\cdots\text{O}$ interactions in **1**, the hydrogen bond lengths range from 2.44 to 2.65 Å (Supplementary Materials, Table S4). The $\text{C-H}\cdots\text{F}$ contacts in **2** are in the range of 2.45–2.55 Å (Supplementary Materials, Table S4).

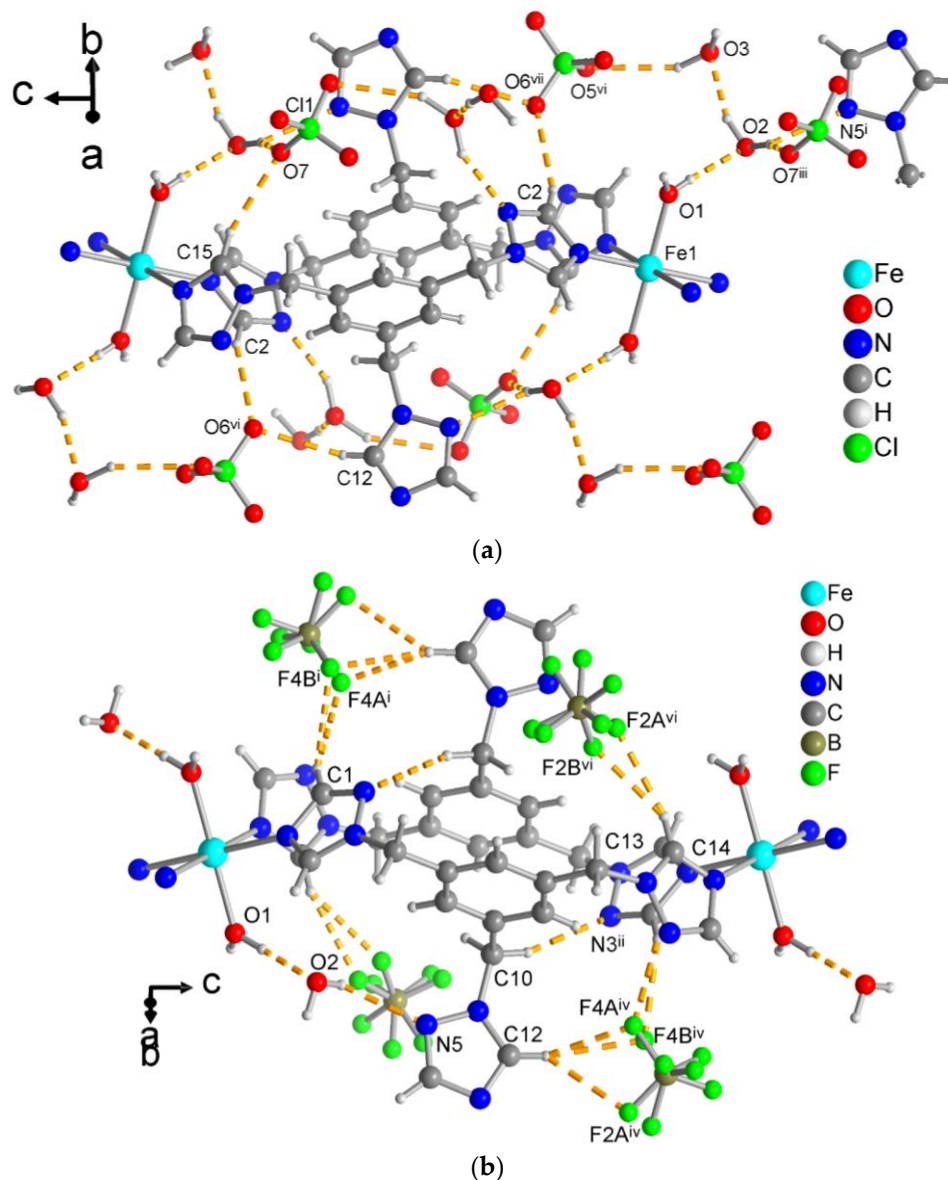


Figure 5. Hydrogen-bonding interactions in compounds (a) **1** and (b) **2** as yellow-orange dashed lines. See Table S4 for details of the H-bond interactions (distances, angles and symmetry operations). Symmetry transformation: (a): $i = -x + 1, -y + 1, -z$; $iii = x, y, z - 1$; $vi = x - 1/2, -y + 3/2, z - 1/2$; $vii = -x + 3/2, y - 1/2, -z + 3/2$. (b): $i = -x + 2, -y + 1, -z + 2$; $ii = -x + 2, -y + 1, -z + 1$; $iv = x, y, z - 1$; $vi = -x + 3/2, y + 1/2, -z + 3/2$.

3.2. Crystal Structure of $[\text{Fe}(\text{NCS})_2(\text{ttmb})_2]$ (**3**)

The X-ray crystallographic analysis reveals that compound **3** crystallizes in the triclinic space group $\text{P}\bar{1}$. The asymmetric unit is composed of one half of an Fe(II) atom (on an inversion center), one ttmb ligand and one coordinated NCS^- anion, as shown in Figure 6. The Fe(II) metal is octahedrally coordinated by six nitrogen donor atoms from four triazole rings in the equatorial plane and two trans-coordinated NCS^- in the axial positions.

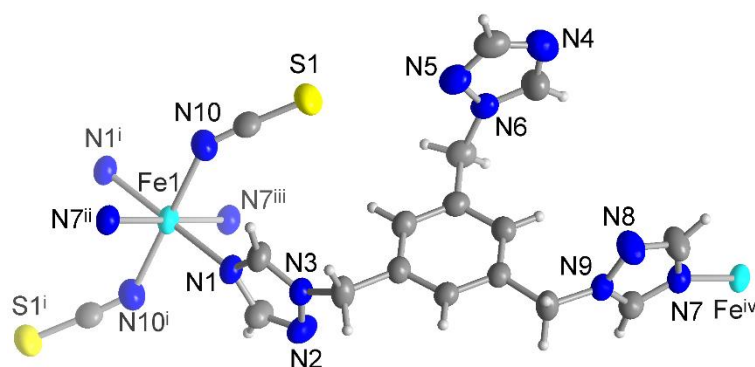


Figure 6. Extended asymmetric unit of compound **3** (50% thermal ellipsoids and H atoms with arbitrary radii). Symmetry transformations: $i = -x + 1, -y + 2, -z$; $ii = x, y + 1, z - 1$; $iii = -x + 1, -y + 1, -z + 1$; $iv = x, y - 1, z + 1$.

The distances of the Fe–N bonds lie between 2.07 and 2.23 Å. Therefore, this compound is also in the HS state. Similar to the structures of compounds **1** and **2**, two Fe(II) atoms are linked by two ttmb linkers in an anti-conformation to form a double-chain structure (Figure 7). The distance between two Fe(II) atoms is 13.79 Å.

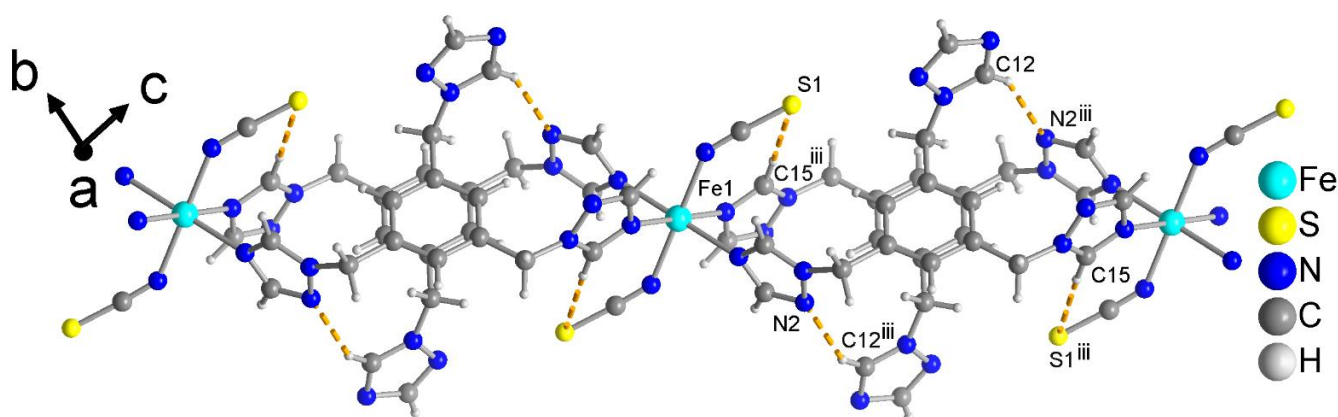


Figure 7. The double chain of compound **3** with the intrachain C–H...N/S hydrogen-bonding interactions as yellow-orange dashed lines. See Table S4 for details of the H-bond interactions (distances and angles). Symmetry transformation: $iii = -x + 1, -y + 1, -z + 1$.

All three compounds form one-dimensional chain structures that interdigitate with the non-coordinated, dangling triazole rings as shown in Figure 8a. The supramolecular organization of the parallel chains is mediated by hydrogen-bonding interactions. In the isostructural compounds **1** and **2**, there are O–H...O and O–H...N interactions from the aqua ligands to the crystal water molecule and to a free triazole-N from the adjacent chain. Further, the crystal water molecule also forms O–H...N bonds to this adjacent chain (Figure 8b). Thus, the chains are interconnected with each other by strong hydrogen bonding. The non-iron-coordinating triazole ring is therefore instrumental for the supramolecular arrangement of the parallel chains. It is also evident, however, that there is no steric hindrance of this ring to an additional metal coordination. Possibly, if less hydrogen-bonding organic solvents are used in the synthesis, this third triazole group could be brought to metal coordination.

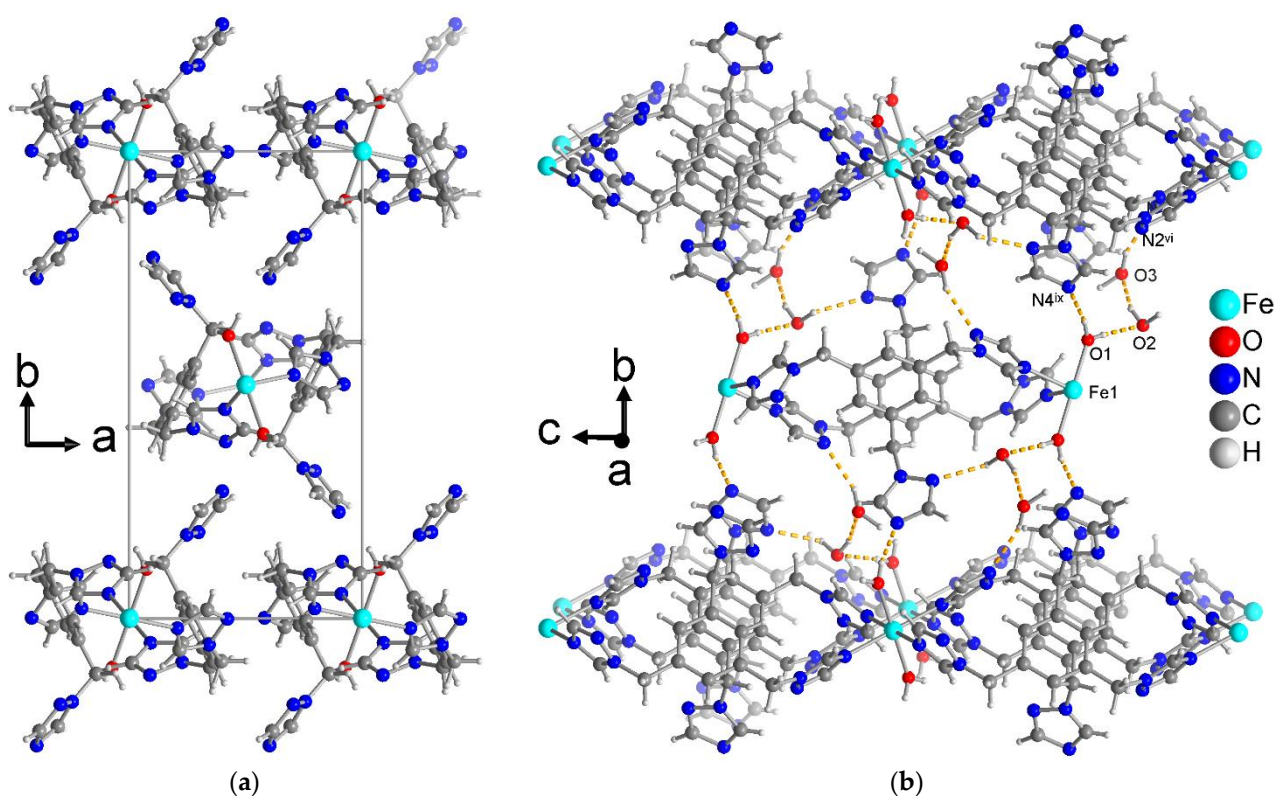


Figure 8. (a) View along the chain directions in compound 1 (isostructural to 2) to depict the interdigitation of the dangling triazole rings (perchlorate ions and crystal water molecules have been omitted for clarity). (b) Hydrogen bonding interactions (yellow-orange dashed lines) between the one-dimensional double chains and the water molecules in the crystal structure of 1 (isostructural to 2) (perchlorate ions have been omitted for clarity). See Table S4 for details of the H-bond interactions (distances and angles). Symmetry transformations: $vi = x - 1/2, -y + 3/2, z - 1/2$; $ix = -x + 3/2, y - 1/2, -z + 1/2$.

In compound 3, the supramolecular packing of the chains is organized by weaker interchain C–H \cdots N/S hydrogen-bonding interactions (Figure 9).

All three compounds were tested for SCO behavior. From the very light-yellow color of compound 1 and colorless compounds 2 and 3, an HS state for d^6 -Fe(II) is apparent. The SCO test was done by cooling the samples to a temperature of 77 K with liquid nitrogen. This method failed to show any change in color to red–violet, which would have indicated a transition to the LS state. Also, ten tons of pressure were applied to the samples using an IR pellet press. Again, no change in color could be detected. In order to observe SCO behavior, rigid ligands are often preferred. Also, balanced cooperative interactions between the Fe centers increase the probability of detecting SCO. This is due to the fact that the M–L bond lengths change during the spin transition and supramolecular interactions then lead to an abrupt spin crossover of all Fe centers in the solid sample [71]. As in the previously synthesized 3D iron(II) frameworks with the 1,1'-(trans-2-butene-1,4-diyl)bis-1,2,4-triazole ligand without SCO effect [72], we can only suggest that the doubly-bridged chain structures of compounds 1–3 are also too rigid within the chain to allow for the shortening of the Fe–N bond lengths when going from the HS to the LS state. In this context, it may be beneficial to use more flexible ligands and also to have single-bridged chain structures.

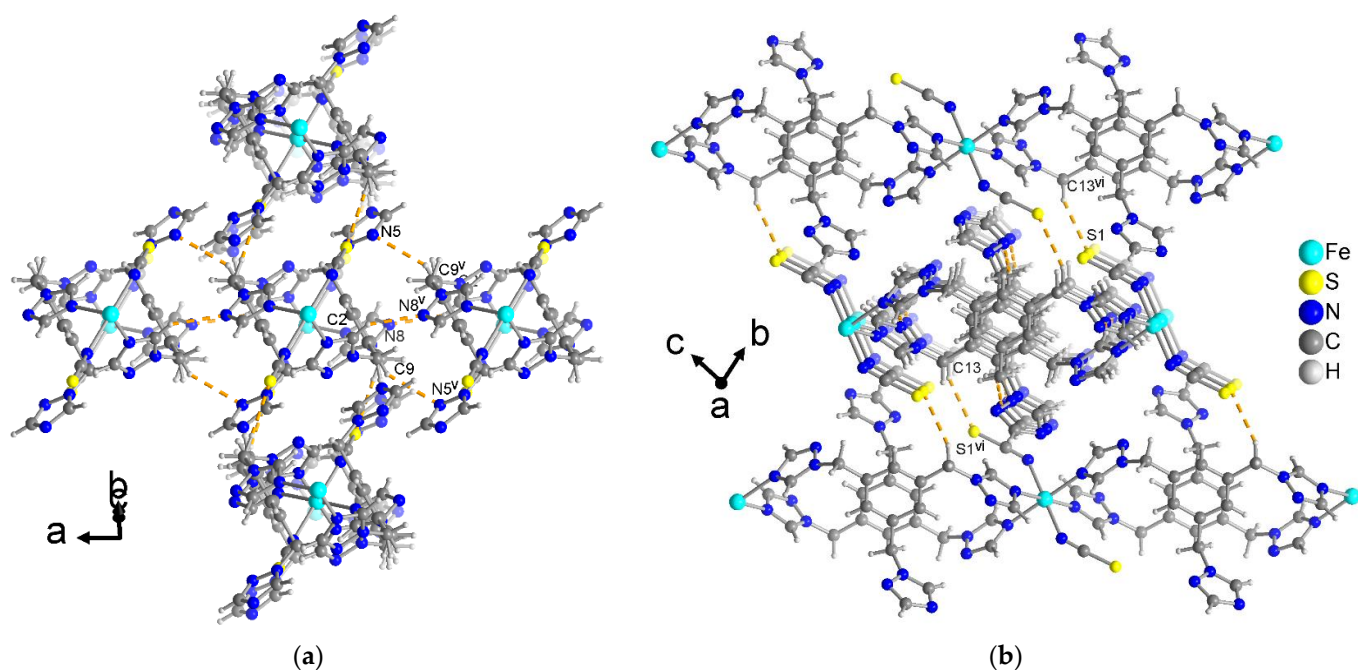


Figure 9. C–H···N/S hydrogen-bonding interactions between the chains in compound **3** (intra-chain C–H···N/S are not shown, cf. Figure 7). (a) The C–H···N interactions connect the chains parallel to the *a* direction. (b) The C–H···S interactions orient the chains perpendicular to the *a* direction. See Table S4 for details of the H-bond interactions (distances and angles). Symmetry transformations: $v = -x, -y + 1, -z + 1$; $vi = x, -y + 1, z$.

4. Conclusions

The new iron(II) coordination polymers [Fe(H₂O)₂(ttmb)₂](ClO₄)₂·4H₂O (**1**), [Fe(H₂O)₂(ttmb)₂](BF₄)₂·4H₂O (**2**), [Fe(NCS)₂(ttmb)₂] (**3**) with the linker 1,3,5-tris((1*H*-1,2,4-triazol-1-yl)methyl)benzene (ttmb) were structurally characterized by single-crystal X-ray diffraction. It was hoped for that the potentially tritopic ttmb linker would utilize its three triazole N-donor groups for metal coordination to form at least 2D if not even 3D coordination networks. Somewhat surprisingly, only two of the triazole groups coordinated to iron. This could have still given a 2D framework if each of the four ttmb linkers around an iron atom would connect to a different iron. Yet, two ttmb linkers each connected to the same iron atom through a double bridge. Subsequently, 1D coordination polymers with a double-chain structure and a 1:2 Fe:ttmb stoichiometry resulted. We note that the metal ions were even offered in excess during the optimized synthesis with a molar M:L ratio of 2:3 for **1** and 2:1 for **2**. We hypothesize that it is not so much the counter anions which exert a templating effect in the structures of **1–3** but the water solvent (or water/ethanol for **2**) from which the compounds were crystallized. Future work using different solvents and also other metal ions for the crystallization should try to invoke the coordination of all triazole groups of the ttmb linker.

Supplementary Materials: The following supporting information can be downloaded at: <https://www.mdpi.com/article/10.3390/cryst13111574/s1>, Section S1: Used Chemicals; Section S2: Ligand analyses; Section S3: Infrared spectra of compounds **1–3**; Section S4: Thermogravimetric analyses of compounds **1–3**; Section S5: Crystal images of compounds **1–3**; Section S6: Crystal data of compounds **1–3**; Section S7: Distortion of the coordination polyhedron of compounds **1–3**; Section S8: Photophysical spectra of ttmb and compounds **1–3**; References [73–77] are cited in the Supplementary Materials.

Author Contributions: Conceptualization, A.L., D.N.J., L.P.C., Y.G. and C.J.; methodology, A.L., D.N.J. and L.P.C.; validation, A.L., D.N.J. and L.P.C.; formal analysis, A.L., D.N.J., T.S. and L.P.C.; investigation, A.L., D.N.J., T.S. and L.P.C.; resources, C.J.; data curation, A.L., D.N.J. and T.S.; writing—original draft preparation, A.L.; writing—review and editing, C.J.; visualization, A.L. and C.J.; supervision, C.J.; project administration, C.J.; funding acquisition, C.J. and Y.G. All authors have read and agreed to the published version of the manuscript.

Funding: Fonds De La Recherche Scientifique—FNRS (PDR T.0095.21, CDR J.0064.23) and the Deutsche Forschungsgemeinschaft (DFG) under grant 440366605 (for the Rigaku diffractometer), grant INST 208/589-1 (for the Bruker diffractometer) and within the Priority Program SPP 1928/2 COORNETs (C.J. grant Ja466/43-1).

Data Availability Statement: The data presented in this study are available on request from the corresponding author. The CCDC numbers 2297073–2297075 for compounds 1–3, respectively, contain the supplementary crystallographic data reported in this paper. These data can be obtained free of charge from the Cambridge Crystallographic Data Centre via www.ccdc.cam.ac.uk/data_request/cif (accessed on 25 September 2023).

Acknowledgments: The authors thank Birgit Tommes for IR measurements, Annette Vollrath and Maximilian Vieten for the photophysical measurements.

Conflicts of Interest: The authors declare no conflict of interest.

References

1. Batten, S.R.; Neville, S.M.; Turner, D.R. *Coordination Polymers. Design, Analysis and Application*; Royal Society of Chemistry: Cambridge, UK, 2009; ISBN 978-0-85404-837-3.
2. Batten, S.R.; Champness, N.R.; Chen, X.-M.; Garcia-Martinez, J.; Kitagawa, S.; Öhrström, L.; O’Keeffe, M.; Suh, M.P.; Reedijk, J. Coordination polymers, metal–organic frameworks and the need for terminology guidelines. *CrystEngComm* **2012**, *14*, 3001. [[CrossRef](#)]
3. Batten, S.R.; Champness, N.R.; Chen, X.-M.; Garcia-Martinez, J.; Kitagawa, S.; Öhrström, L.; O’Keeffe, M.; Paik Suh, M.; Reedijk, J. Terminology of metal–organic frameworks and coordination polymers (IUPAC Recommendations 2013). *Pure Appl. Chem.* **2013**, *85*, 1715–1724. [[CrossRef](#)]
4. Kuznetsova, A.; Matveevskaya, V.; Pavlov, D.; Yakunenkova, A.; Potapov, A. Coordination Polymers Based on Highly Emissive Ligands: Synthesis and Functional Properties. *Materials* **2020**, *13*, 2699. [[CrossRef](#)] [[PubMed](#)]
5. Leong, W.L.; Vittal, J.J. One-dimensional coordination polymers: Complexity and diversity in structures, properties, and applications. *Chem. Rev.* **2011**, *111*, 688–764. [[CrossRef](#)]
6. Kitagawa, S.; Kitaura, R.; Noro, S. Functional porous coordination polymers. *Angew. Chem. Int. Ed.* **2004**, *43*, 2334–2375. [[CrossRef](#)]
7. Robin, A.Y.; Fromm, K.M. Coordination polymer networks with O- and N-donors: What they are, why and how they are made. *Coord. Chem. Rev.* **2006**, *250*, 2127–2157. [[CrossRef](#)]
8. Naik, A.D.; Dirtu, M.M.; Railliet, A.P.; Marchand-Brynaert, J.; Garcia, Y. Coordination Polymers and Metal Organic Frameworks Derived from 1,2,4-Triazole Amino Acid Linkers. *Polymers* **2011**, *3*, 1750–1775. [[CrossRef](#)]
9. Hoskins, B.F.; Robson, R. Infinite polymeric frameworks consisting of three dimensionally linked rod-like segments. *J. Am. Chem. Soc.* **1989**, *111*, 5962–5964. [[CrossRef](#)]
10. Horike, S.; Shimomura, S.; Kitagawa, S. Soft porous crystals. *Nat. Chem.* **2009**, *1*, 695–704. [[CrossRef](#)]
11. Kitagawa, S.; Noro, S.; Nakamura, T. Pore surface engineering of microporous coordination polymers. *Chem. Commun.* **2006**, 701–707. [[CrossRef](#)]
12. Lehn, J.-M. *Supramolecular Chemistry: Concepts and Perspectives*; A Personal Account Built upon the George Fisher Baker Lectures in Chemistry at Cornell University and Lezioni Lincee, Accademia Nazionale dei Lincei, Roma; VCH: Weinheim, Germany; New York, NY, USA, 1995; ISBN 3527293124.
13. Mu, Y.; Han, G.; Ji, S.; Hou, H.; Fan, Y. Coordination polymers based on a flexible bis(triazole) ligand and aromatic polycarboxylate anions: Syntheses, topological structures and photoluminescent properties. *CrystEngComm* **2011**, *13*, 5943. [[CrossRef](#)]
14. Du, M.; Bu, X.-H.; Huang, Z.; Chen, S.-T.; Guo, Y.-M.; Diaz, C.; Ribas, J. From metallacyclophanes to 1-D coordination polymers: Role of anions in self-assembly processes of copper(II) and 2,5-bis(3-pyridyl)-1,3,4-oxadiazole. *Inorg. Chem.* **2003**, *42*, 552–559. [[CrossRef](#)] [[PubMed](#)]
15. Chand, D.K.; Biradha, K.; Fujita, M.; Sakamoto, S.; Yamaguchi, K. A molecular sphere of octahedral symmetry. *Chem. Commun.* **2002**, 2486–2487. [[CrossRef](#)]
16. Friese, V.A.; Kurth, D.G. From coordination complexes to coordination polymers through self-assembly. *Curr. Opin. Colloid Interface Sci.* **2009**, *14*, 81–93. [[CrossRef](#)]
17. Li, W.; Kim, Y.; Li, J.; Lee, M. Dynamic self-assembly of coordination polymers in aqueous solution. *Soft Matter* **2014**, *10*, 5231–5242. [[CrossRef](#)]

18. Liu, H.-L.; Sun, W.-Y.; Zhu, H.-L.; Yu, K.-B.; Tang, W.-X. A two-dimensional network constructed via 72-membered heart-shaped macrocycles, a copper(II) complex with 1,3,5-tris(imidazol-1-ylmethyl)-2,4,6-trimethylbenzene and diethylenetriamine ligands. *Inorg. Chim. Acta* **1999**, *295*, 129–135. [[CrossRef](#)]
19. Shi, X.; Tan, D.; Liu, Y.; Liang, G.; Zhang, X. Syntheses, structures and fluorescence properties of two novel polymers based on a flexible tripodal ligand 1,3,5-tris((1H-1,2,4-triazol-1-yl)methyl)benzene. *J. Mol. Struct.* **2014**, *1074*, 134–139. [[CrossRef](#)]
20. Shi, X.; Zhang, X.; Li, X.; Hou, H.; Fan, Y. Structure analysis and catalytic property of a microporous framework based on a flexible tripodal ligand with novel conformations. *J. Mol. Struct.* **2011**, *996*, 110–114. [[CrossRef](#)]
21. Yin, X.-J.; Zhou, X.-H.; Gu, Z.-G.; Zuo, J.-L.; You, X.-Z. Syntheses and physical properties of three-dimensional coordination polymers with the flexible tripodal ligand 1,3,5-tris(1,2,4-triazol-1-ylmethyl)benzene. *Inorg. Chem. Commun.* **2009**, *12*, 548–551. [[CrossRef](#)]
22. Shi, Z.; Pan, Z.; Zhang, C.; Zheng, H. Syntheses, structures, and properties of six cobalt(II) complexes based on a tripodal tris(4-(1H-1,2,4-triazol-1-yl)phenyl)amine ligand. *Dalton Trans.* **2015**, *44*, 16854–16864. [[CrossRef](#)]
23. Li, B.Z.; Liu, X.G.; Wang, Z.H.; Li, B.L.; Zhang, Y. A novel two-dimensional network cadmium(II) coordination polymer containing one 1,4-bis(1,2,4-triazol-1-yl)butane and double dicyanamide bridges. *Acta Crystallogr. C* **2006**, *62*, m10-2. [[CrossRef](#)] [[PubMed](#)]
24. Woschko, D.; Millan, S.; Ceyran, M.-A.; Oestreich, R.; Janiak, C. Synthesis of a Chiral 3,6T22-Zn-MOF with a T-Shaped Bifunctional Pyrazole-Isophthalate Ligand Following the Principles of the Supramolecular Building Layer Approach. *Molecules* **2022**, *27*, 5374. [[CrossRef](#)] [[PubMed](#)]
25. Aromí, G.; Barrios, L.A.; Roubeau, O.; Gamez, P. Triazoles and tetrazoles: Prime ligands to generate remarkable coordination materials. *Coord. Chem. Rev.* **2011**, *255*, 485–546. [[CrossRef](#)]
26. Haasnoot, J.G. Mononuclear, oligonuclear and polynuclear metal coordination compounds with 1,2,4-triazole derivatives as ligands. *Coord. Chem. Rev.* **2000**, *200–202*, 131–185. [[CrossRef](#)]
27. Garcia, Y.; Adarsh, N.N.; Naik, A.D. Crystal engineering of Fe(II) spin crossover coordination polymers derived from triazole or tetrazole ligands. *Chimia* **2013**, *67*, 411–418. [[CrossRef](#)]
28. Ding, B.; Yi, L.; Cheng, P.; Liao, D.-Z.; Yan, S.-P. Synthesis and characterization of a 3D coordination polymer based on trinuclear triangular CuII as secondary building units. *Inorg. Chem.* **2006**, *45*, 5799–5803. [[CrossRef](#)]
29. Ouellette, W.; Liu, H.; O'Connor, C.J.; Zubieta, J. Solid-state coordination chemistry of copper(II) tetrazolates: Anion control of frameworks constructed from trinuclear copper(II) building blocks. *Inorg. Chem.* **2009**, *48*, 4655–4657. [[CrossRef](#)]
30. Ouellette, W.; Hudson, B.S.; Zubieta, J. Hydrothermal and structural chemistry of the zinc(II)- and cadmium(II)-1,2,4-triazolate systems. *Inorg. Chem.* **2007**, *46*, 4887–4904. [[CrossRef](#)]
31. Zhang, J.-P.; Chen, X.-M. Crystal engineering of binary metal imidazolate and triazolate frameworks. *Chem. Commun.* **2006**, 1689–16990. [[CrossRef](#)]
32. Wang, H.-P.; Wang, H.-L.; Li, B.-L. Synthesis, Structure, Luminescence and Thermal Stability Properties of a New (3,4)-Connected 2D Zn Coordination Polymer. *J. Struct. Chem.* **2020**, *10*, 1835–1840. [[CrossRef](#)]
33. Li, H.; Liu, G.; Liu, T.T.; Zhang, H.Y.; Yue, F.; Wang, J.D. Syntheses of triazole-bridged cadmium coordination polymer with luminescence properties. *Russ. J. Coord. Chem.* **2011**, *37*, 8–11. [[CrossRef](#)]
34. Lin, H.-Y.; Luan, J.; Wang, X.-L.; Zhang, J.-W.; Liu, G.-C.; Tian, A.-X. Construction and properties of cobalt(ii)/copper(ii) coordination polymers based on N-donor ligands and polycarboxylates mixed ligands. *RSC Adv.* **2014**, *4*, 62430–62445. [[CrossRef](#)]
35. Schweifer, J.; Weinberger, P.; Mereiter, K.; Boca, M.; Reichl, C.; Wiesinger, G.; Hilscher, G.; van Koningsbruggen, P.J.; Koojiman, H.; Grunert, M.; et al. *catena*-[μ -Tris(1,2-bis(tetrazol-1-yl)ethane-N4,N4')iron(II)] bis(tetrafluoroborate): Synthesis, structure, spectroscopic and magnetic characterization of a chain-type coordination polymer spin-crossover compound. *Inorg. Chim. Acta* **2002**, *339*, 297–306. [[CrossRef](#)]
36. Absmeier, A.; Bartel, M.; Carbonera, C.; Jameson, G.N.L.; Werner, F.; Reissner, M.; Caneschi, A.; Létard, J.-F.; Linert, W. Mutual Influence of Spacer Length and Noncoordinating Anions on Thermal and Light-Induced Spin-Crossover Properties of Iron(II)- α,ω -Bis(tetrazol-1-yl)alkane Coordination Polymers. *Eur. J. Inorg. Chem.* **2007**, *2007*, 3047–3054. [[CrossRef](#)]
37. Li, D.-P.; Zhou, X.-H.; Liang, X.-Q.; Li, C.-H.; Chen, C.; Liu, J.; You, X.-Z. Novel Structural Diversity of Triazolate-Based Coordination Polymers Generated Solvothermally with Anions. *Cryst. Growth Des.* **2010**, *10*, 2136–2145. [[CrossRef](#)]
38. Schottel, B.L.; Chifotides, H.T.; Shatruk, M.; Chouai, A.; Pérez, L.M.; Bacsá, J.; Dunbar, K.R. Anion- π interactions as controlling elements in self-assembly reactions of Ag(I) complexes with π -acidic aromatic rings. *J. Am. Chem. Soc.* **2006**, *128*, 5895–5912. [[CrossRef](#)]
39. Busch, D.H. Structural Definition of Chemical Templates and the Prediction of New and Unusual Materials. *Am. Chem. Soc.* **1992**, *12*, 389–395. [[CrossRef](#)]
40. Anderson, S.; Anderson, H.L.; Sanders, J.K.M. Expanding roles for templates in synthesis. *Acc. Chem. Res.* **1993**, *26*, 469–475. [[CrossRef](#)]
41. Zhu, X.; Wang, L.-Y.; Liu, X.-G.; Wang, J.; Li, B.-L.; Li, H.-Y. Structural versatility of seven copper(ii) coordination polymers constructed with the long flexible ligand 1,4-bis(1,2,4-triazol-1-yl)butane. *CrystEngComm* **2011**, *13*, 6090. [[CrossRef](#)]
42. Tanaka, D.; Kitagawa, S. Template Effects in Porous Coordination Polymers. *Chem. Mater.* **2008**, *20*, 922–931. [[CrossRef](#)]
43. Halper, S.R.; Do, L.; Stork, J.R.; Cohen, S.M. Topological Control in Heterometallic Metal-Organic Frameworks by Anion Templating and Metalloligand Design. *J. Am. Chem. Soc.* **2006**, *128*, 15255–15268. [[CrossRef](#)] [[PubMed](#)]

44. Beer, P.D.; Gale, P.A. Anion Recognition and Sensing: The State of the Art and Future Perspectives. *Angew. Chem. Int. Ed.* **2001**, *40*, 486–516. [[CrossRef](#)]
45. Huang, X.-C.; Zhang, J.-P.; Chen, X.-M. A new route to supramolecular isomers via molecular templating: Nanosized molecular polygons of copper(I) 2-methylimidazolates. *J. Am. Chem. Soc.* **2004**, *126*, 13218–13219. [[CrossRef](#)] [[PubMed](#)]
46. Huang, X.-C.; Zhang, J.-P.; Lin, Y.-Y.; Chen, X.-M. Triple-stranded helices and zigzag chains of copper(I) 2-ethylimidazolate: Solvent polarity-induced supramolecular isomerism. *Chem. Commun.* **2005**, 2232–2234. [[CrossRef](#)] [[PubMed](#)]
47. Vilar, R. Anion-templated synthesis. *Angew. Chem. Int. Ed Engl.* **2003**, *42*, 1460–1477. [[CrossRef](#)] [[PubMed](#)]
48. Wang, H.; Feng, Y.; Liang, N.; Li, B.; Zhang, Y. Two nickel coordination polymers with flexible ligand 1,3,5-tri(1,2,4-triazol-1-ylmethyl)-2,4,6-trimethylbenzene. *Inorg. Chem. Commun.* **2009**, *12*, 1161–1163. [[CrossRef](#)]
49. Gimeno, N.; Vilar, R. Anions as templates in coordination and supramolecular chemistry. *Coord. Chem. Rev.* **2006**, *250*, 3161–3189. [[CrossRef](#)]
50. Kim, H.-J.; Zin, W.-C.; Lee, M. Anion-directed self-assembly of coordination polymer into tunable secondary structure. *J. Am. Chem. Soc.* **2004**, *126*, 7009–7014. [[CrossRef](#)]
51. Lankshear, M.D.; Beer, P.D. Strategic anion templation. *Coord. Chem. Rev.* **2006**, *250*, 3142–3160. [[CrossRef](#)]
52. Shi, Q.; Cao, R.; Sun, D.-F.; Hong, M.-C.; Liang, Y.-C. Solvothermal syntheses and crystal structures of two metal coordination polymers with double-chain structures. *Polyhedron* **2001**, *20*, 3287–3293. [[CrossRef](#)]
53. Gütllich, P.; Goodwin, H.A. *Spin Crossover—An Overall Perspective*; Topics in Current Chemistry; Springer: Berlin/Heidelberg, Germany, 2004; pp. 1–47. [[CrossRef](#)]
54. Gütllich, P.; Gaspar, A.B.; Garcia, Y. Spin state switching in iron coordination compounds. *Beilstein J. Org. Chem.* **2013**, *9*, 342–391. [[CrossRef](#)]
55. Brooker, S. Spin crossover with thermal hysteresis: Practicalities and lessons learnt. *Chem. Soc. Rev.* **2015**, *44*, 2880–2892. [[CrossRef](#)]
56. Real, J.A.; Gaspar, A.B.; Niel, V.; Munoy, M.C. Communication between iron(II) building blocks in cooperative spin transition phenomena. *Coord. Chem. Rev.* **2003**, *236*, 121–141. [[CrossRef](#)]
57. Macrae, C.F.; Sovago, I.; Cottrell, S.J.; Galek, P.T.A.; McCabe, P.; Pidcock, E.; Platings, M.; Shields, G.P.; Stevens, J.S.; Towler, M.; et al. Mercury 4.0: From visualization to analysis, design and prediction. *J. Appl. Crystallogr.* **2020**, *53*, 226–235. [[CrossRef](#)]
58. CrysAlisPro. *Rigaku Oxford Diffraction*; Release 1.171.40.103a; Agilent; Agilent Technologies Ltd.: Yarnton, UK, 2014.
59. APEX2. *Data Collection Program for the CCD Area-Detector System, Version 2.1-0*; Bruker Analytical X-ray Systems: Madison, WI, USA, 1997–2014.
60. SAINT. *Data Reduction and Frame Integration Program for the CCD Area-Detector System*; Bruker Analytical X-ray Systems: Madison, WI, USA, 1997–2014.
61. Sheldrick, G.M. *SADABS: Area-Detector Absorption Correction*; University of Göttingen: Göttingen, Germany, 1996.
62. Dolomanov, O.V.; Bourhis, L.J.; Gildea, R.J.; Howard, J.A.K.; Puschmann, H. OLEX2: A complete structure solution, refinement and analysis program. *J. Appl. Crystallogr.* **2009**, *42*, 339–341. [[CrossRef](#)]
63. Sheldrick, G.M. SHELXT—Integrated space-group and crystal-structure determination. *Acta Crystallogr. A* **2015**, *71*, 3–8. [[CrossRef](#)] [[PubMed](#)]
64. Sheldrick, G.M. Crystal structure refinement with SHELXL. *Acta Crystallogr. C* **2015**, *71*, 3–8. [[CrossRef](#)] [[PubMed](#)]
65. Brandenburg, K. *Diamond, Version 4.5*; Crystal and Molecular Structure Visualization, Crystal Impact; K. Brandenburg & H. Putz Gbr: Bonn, Germany, 2009–2022.
66. Shang, Q.; Zeng, T.; Gao, K.; Liu, N.; Cheng, Q.; Liao, G.; Pan, Z.; Zhou, H. A novel nitrogen heterocyclic ligand-based MOF: Synthesis, characterization and photocatalytic properties. *New J. Chem.* **2019**, *43*, 16595–16603. [[CrossRef](#)]
67. Garcia, Y.; Bravic, G.; Gieck, C.; Chasseau, D.; Tremel, W.; Gütllich, P. Crystal structure, magnetic properties, and 57Fe Mössbauer spectroscopy of the two-dimensional coordination polymers M(1,2-bis(1,2,4-triazol-4-yl)ethane)2(NCS)2 (MII = Fe, Co). *Inorg. Chem.* **2005**, *44*, 9723–9730. [[CrossRef](#)]
68. Lavrenova, L.G.; Yudina, N.G.; Ikorskii, V.N.; Varnek, V.A.; Oglezneva, I.M.; Larionov, S.V. Spin-crossover and thermochromism in complexes of iron(II) iodide and thiocyanate with 4-amino-1,2,4-triazole. *Polyhedron* **1995**, *14*, 1333–1337. [[CrossRef](#)]
69. Hesse, M.; Meier, H.; Zeeh, B.; Bienz, S.; Bigler, L.; Fox, T. *Spektroskopische Methoden in der Organischen Chemie*; 8 Auflage; Georg Thieme Verlag: Stuttgart, Germany, 2012; ISBN 9783135761084.
70. Moll, J.; Förster, C.; König, A.; Carrella, L.M.; Wagner, M.; Panthöfer, M.; Möller, A.; Rentschler, E.; Heinze, K. Panchromatic Absorption and Oxidation of an Iron(II) Spin Crossover Complex. *Inorg. Chem.* **2022**, *61*, 1659–1671. [[CrossRef](#)] [[PubMed](#)]
71. Weber, B. Spin crossover complexes with N4O2 coordination sphere—The influence of covalent linkers on cooperative interactions. *Coord. Chem. Rev.* **2009**, *253*, 2432–2449. [[CrossRef](#)]
72. Jordan, D.N.; Straßburg, P.G.; Woschko, D.; Carrella, L.M.; Cuignet, L.P.; Eickmeier, K.; Dronskowski, R.; Garcia, Y.; Rentschler, E.; Janiak, C. Interpenetration Phenomena via Anion Template Effects in Fe(II) and Co(II) Coordination Networks with a Bis-(1,2,4-triazole) Ligand. *Polymers* **2023**, *15*, 3286. [[CrossRef](#)] [[PubMed](#)]
73. Ketkaew, R.; Tantirungrotechai, Y.; Harding, P.; Chastanet, G.; Guionneau, P.; Marchivie, M.; Harding, D.J. OctaDist: A tool for calculating distortion parameters in spin crossover and coordination complexes. *Dalton Trans.* **2021**, *50*, 1086–1096. [[CrossRef](#)]
74. Buron-Le Cointe, M.; Hébert, J.; Baldé, C.; Moisan, N.; Toupet, L.; Guionneau, P.; Létard, J.F.; Freysz, E.; Cailleau, H.; Collet, E. Intermolecular control of thermoswitching and photoswitching phenomena in two spin-crossover polymorphs. *Phys. Rev. B* **2012**, *85*, 064114. [[CrossRef](#)]

75. McCusker, J.K.; Rheingold, A.L.; Hendrickson, D.N. Variable-Temperature Studies of Laser-Initiated $^5T_2 \rightarrow ^1A_1$ Intersystem Crossing in Spin-Crossover Complexes: Empirical Correlations between Activation Parameters and Ligand Structure in a Series of Polypyridyl Ferrous Complexes. *Inorg. Chem.* **1996**, *35*, 2100–2112. [[CrossRef](#)]
76. Marchivie, M.; Guionneau, P.; Létard, J.F.; Chasseau, D. Photo-induced spin-transition: The role of the iron(II) environment distortion. *Acta Crystallogr. B* **2005**, *61*, 25–28. [[CrossRef](#)]
77. Avila, Y.; Pérez, O.; Sánchez, L.; Vázquez, M.C.; Mojica, R.; González, M.; Ávila, M.; Rodríguez-Hernández, J.; Reguera, E. Spin crossover in Hofmann-like coordination polymers. Effect of the axial ligand substituent and its position. *New J. Chem.* **2023**, *47*, 10781–10795. [[CrossRef](#)]

Disclaimer/Publisher's Note: The statements, opinions and data contained in all publications are solely those of the individual author(s) and contributor(s) and not of MDPI and/or the editor(s). MDPI and/or the editor(s) disclaim responsibility for any injury to people or property resulting from any ideas, methods, instructions or products referred to in the content.